J. Coat. Technol. Res.
https://doi.org/10.1007/s11998-024-00954-z

Effect of silica nanocomposite modified with some polythiophene derivations on characteristics and properties of waterborne acrylic coatings

Duong Thi Thuy Nguyen, Dai Ba Do, Thinh Huu Nguyen, Chinh Thuy Nguyen, Thai Xuan Nguyen, Hung Phi Dao, Hoang Thai, Linh Ngoc Nguyen, Manh Quoc Vu, Trung Quoc Vu

Received: 1 November 2023 / Revised: 29 March 2024 / Accepted: 30 March 2024

Abstract In this study, we utilized nanocomposites prepared from nanosilica (SiO_2) and various polythiophene derivatives as enhancement additives for acrylic coatings. The nanocomposites were synthesized in a nitrogen environment using $FeCl_3$ as a catalyst in a chloroform solvent. The weight ratio of nanosilica to monomers was 2/1, specifically for the compounds (5-benzo[*d*]thiazol-2-yl)-7-methoxy-2-(thiophen-3-yl) benzo[*d*]oxazole (P1), 3-(2-benzothiazolyl)thiophene (P2), and 5-(benzo[*d*]thiazol-2-yl)-2-(thiophene-3-yl)benzo[*d*]oxazole (P3). Analysis techniques including IR, TGA, SEM, and UV–Vis were employed to demonstrate the formation of polythiophenes on the surface of the nanosilica. The presence of polythiophenes on the nanosilica broadened the UV absorption region. Upon adding the nanocomposites to acrylic coatings, the UV absorption intensity of the coatings was increased. Notably, the coating containing SiO_2-P3 nanocomposite exhibited the highest abrasion resistance among all the investigated samples. By varying the content of SiO_2-P3 nanocomposite, we observed enhanced abrasion resistance, adhesion, pencil hardness, and gloss of the acrylic coating. The maximum values were achieved when the content of SiO_2-P3 nanoparticles was 2 wt.%. The SiO_2-P3 nanoparticles were uniformly dispersed in the acrylic coatings, leading to an improvement in the coating's sunlight-reflective ability. Consequently, the acrylic/SiO_2-P3 nanocomposite coatings exhibited potential for outdoor applications, particularly as UV-resistant coatings.

Keywords Polythiophene derivatives, Benzo[*d*]thiazole heterocyclic, Acrylic emulsion resin, Abrasion resistance, Heat reflective

D. T. T. Nguyen, C. T. Nguyen, T. X. Nguyen, H. P. Dao, H. Thai
Institute for Tropical Technology, Vietnam Academy of Science and Technology, 18 Hoang Quoc Viet, Cau Giay, Ha Noi 100000, Viet Nam

D. T. T. Nguyen, C. T. Nguyen, H. Thai
Graduate University of Science and Technology, Vietnam Academy of Science and Technology, 18 Hoang Quoc Viet, Cau Giay, Ha Noi 100000, Viet Nam

D. B. Do
Nguyen Trai High School, 50 Nam Cao, Ba Dinh, Ha Noi 100000, Viet Nam

D. B. Do, T. H. Nguyen, T. Q. Vu (✉)
Faculty of Chemistry, Hanoi National University of Education, 136 Xuan Thuy, Cau Giay, Ha Noi 100000, Viet Nam
e-mail: trungvq@hnue.edu.vn

L. N. Nguyen, M. Q. Vu
Thanh Do University, Kim Chung, Hoai Duc, Ha Noi 100000, Viet Nam

Introduction

Polythiophene (PTh) and its derivatives have undergone extensive research and found diverse applications in various fields over the past few decades. This is primarily due to their remarkable semiconductor, electronic, and optical properties, as well as their favorable mechanical characteristics.[1–3] However, the PTh suffers from limited solubility in both organic solvents and aqueous solutions. To overcome this limitation, active substituents are introduced to the thiophene ring. These substituents enhance the solubility and conductivity of the PThs in commonly used organic solvents and improve their compatibility with polymeric substrates. By modifying the substituents, the key properties of these materials, such as conductivity, optical properties, magnetic properties, size, and shape, can be easily adjusted.[1,2]

Published online: 17 June 2024

Depending on the level of doping, the PThs can exhibit characteristics of conductors or semiconductors, resembling metallic elements. The PThs doped at the metallic level have potential applications in batteries, electrochemical or smart windows, antistatic coatings, and various sensors.[3,4] On the other hand, when the PThs are synthesized in their semiconductor form, they demonstrate electrical and optical properties similar to those of inorganic semiconductors. This makes them suitable for a wide range of applications, including solar cells, field-effect organic transistors, organic light-emitting diodes, and field-effect transistors (o-FETs).[3,4] Moreover, combining conductive polymers like the PThs with other polymers enables the creation of new materials with enhanced properties. In addition, the utilization of nanosilica as an additive to enhance coatings has been increasingly explored in recent years. The incorporation of nanosilica into polymer coatings has shown considerable benefits in improving their mechanical properties, including hardness, scratch resistance, and wear resistance. Furthermore, nanosilica can enhance the barrier properties of coatings against gas and water vapor permeation.[5,6] The dispersion of nanosilica within the polymer matrix plays a crucial role in determining the performance of nanocomposite coatings. Effective dispersion is essential to prevent nanoparticle agglomeration and the formation of defects, which can otherwise compromise the overall performance of the coating.[7] A core-shell structure has been suggested for nanocomposites based on TiO_2 and polythiophene.[8,9] TiO_2 used in this case is n-type semiconductor. The nanocomposites have been electrophoretic deposited by cathodic preparation to form thin films.

Acrylic emulsion resins have garnered attention for their potential in the development of pressure-sensitive adhesives (PSAs) due to their advantageous properties, including high adhesive strength, good cohesion, and low tack.[10–12] The research focuses on optimizing the properties of acrylic emulsion PSAs by modifying the chemical composition of the emulsion polymers, incorporating different monomers, and incorporating functional additives such as tackifiers, crosslinking agents, and plasticizers. Furthermore, the utilization of nanomaterials like silica nanoparticles, graphene oxide, and carbon nanotubes as reinforcing agents in acrylic emulsion PSAs has been investigated, yielding promising results in enhancing the adhesive strength and durability of the PSAs.[13–16] These advancements have led to the extensive application of acrylic emulsion-based PSAs in various domains, including tapes, labels, and medical adhesives.

Recent studies have indicated that the dispersion and compatibility of nanosilica in a polymer matrix can be enhanced through the use of polymer-grafted nanosilica or silan-grafted nanosilica.[17–25] For instance, the grafting of poly(methyl methacrylate) (PMMA) onto nanosilica has been found to significantly improve its dispersibility in PMMA matrix, leading to improved mechanical properties in comparison with unmodified nanosilica.[22] Likewise, the grafting of poly(ethylene oxide) (PEO) onto nanosilica has demonstrated enhanced dispersibility and adhesion of nanosilica in polyurethane coatings.[26] These findings highlight that surface modification of nanosilica through polymer grafting presents a promising approach to enhance the performance of nanosilica-polymer nanocomposites.

In the context of the previous paragraphs, the mentioned study investigated the use of nanosilica and polythiophenes as additives to enhance acrylic coatings. Through the in situ synthesis of polythiophenes on the surface of nanosilica, nanocomposites formed were powdery, exhibiting improved UV absorption properties. Nanosilica and polythiophenes can synergistically form a novel nanocomposite with remarkable UV absorbance capabilities. The nanosilica exhibits UV absorption in the short wavelength range, while polythiophene derivatives containing benzo[*d*]thiazol heterocycle effectively shield UV rays across a broader wavelength spectrum.[27] In our previous studies, the green synthesis and crystal structure of polythiophene derivatives containing benzo[*d*]thiazol heterocycle have been reported.[27–29] Thus, this study aims to utilize nanocomposites comprising silica nanoparticles and polythiophene derivatives as reinforcing additives for acrylic coatings. The nanocomposites were synthesized using a chemical polymerization method involving the 3-thiophenecarbaldehyde monomer, $FeCl_3$ catalyst, and silicon oxide nanoparticles. The investigation further assessed and discussed the mechanical and thermal properties, morphology, and UV absorption capacity of the resultant acrylic coating. The incorporation of SiO_2-polythiophene derivatives containing benzo[*d*]thiazol heterocycle nanocomposite into the acrylic coatings resulted in enhanced UV absorption intensity and abrasion resistance. Moreover, the dispersion of SiO_2-polythiophene derivatives containing benzo[*d*]thiazol heterocycle nanoparticles within the acrylic coating contributed to an improved sunlight-reflective ability. These findings highlight the potential of nanosilica-based nanocomposites in the development of high-performance coatings with enhanced mechanical and optical properties.

Experimental

Materials

3-Thiophenecarbaldehyde (98%) and 2-aminothiophenol (99%) were obtained from Sigma-Aldrich, while 4-hydroxybenzaldehyde (98%) was sourced from Merck. Acetic acid (99.95%), sulfuric acid (98%), hydrochloric acid (38%), ethanol (99.8%), and methanol (99.8%) were provided by Nanjing Chemical Reagent Co., China. Iron powder (98%) and chloroform were supplied by Analytical Reagent, and iron(III) chloride (98%) was purchased from Merck. Silicon dioxide

nanoparticles (size 20–30 nm, 99%) were ordered from Sigma-Aldrich. The acrylic emulsion resin used in the study was Plextol R4152, a commercial product with a solid content of 48.0–50.0%, a pH range of 7.0–8.5, and a viscosity of less than 3000 cps at 25°C.

The synthesis of polythiophene/SiO_2 nanocomposite

The polythiophene/SiO_2 nanocomposite was synthesized using a chemical polymerization method. At the first, the monomers (**1**), (**2**), and (**3**) were prepared as per the procedures described in a previous study.[27] Chloroform (40 mL) was added to a reaction vessel, and nitrogen gas was used to expel air. Anhydrous iron (III) chloride was introduced, followed by the addition of silicon oxide. The monomer (**1**), (**2**), or (**3**) was dissolved in chloroform with a monomer: SiO_2 weight ratio of 1:2. The chemical polymerization was conducted for 24 h. Afterward, methanol (10 mL) was added with stirring for 15 min. The resulting precipitate was filtered, washed with ethanol, rinsed with deionized water, and extracted using a Soxhlet apparatus. The nanocomposites obtained were named SiO_2-P1, SiO_2-P2, and SiO_2-P3, corresponding to the respective monomers used, (**1**), (**2**), and (**3**), respectively. SiO_2-P1 appeared as a brown–black precipitate, SiO_2-P2 as brown–red, and SiO_2-P3 as brown in color.

Fabrication of nanocomposite coating

In this study, the nanocomposite particles were incorporated into an acrylic coating. To achieve this, 0.02 g of the nanocomposite particles was dispersed in 0.2 g of distilled water using an ultrasonic bath. The resulting mixture was then combined with 2 g of the R4152 acrylic resin and stirred for 15 min at room temperature. Subsequently, the mixture was applied to cleaned surfaces using an Erichsen Film Applicator and left to dry for 7 days at room temperature. Prior to each test, the samples were further stabilized at 25°C and 60% relative humidity for 24 h.

To assess the influence of the nanocomposite content on the properties of the acrylic coating, different concentrations of the nanocomposite were employed at 1%, 2%, 3%, and 5% (w/w) relative to the weight of the acrylic resin. The control sample, used for comparison, was prepared under the same conditions but incorporated only 2 wt.% of silicon dioxide nanoparticles into the acrylic coating.

Characterization

FTIR spectroscopy

The IR spectra of the samples were obtained using an infrared spectroscopy instrument (IR Nicolet iS10, Thermo Scientific, USA). For the powder samples, pellets were prepared by mixing the samples with KBr at a mass ratio of 1:50 to record the transmittance spectra. On the other hand, the film samples were analyzed using ATR-IR spectroscopy.

Field emission scanning electron microscopy (FE-SEM) and high-resolution transmission electron microscopy (HR-TEM)

The morphology of the samples was examined using a field emission scanning electron microscope (SEM S-4800, Hitachi, Japan). Prior to image capture, the samples were coated with Pt to enhance the resolution of the images. HR-TEM images of samples were taken on a JEM-2100 Electron Microscope (Jeol, Japan).

Thermo-gravimetric analysis (TGA)

Thermo-gravimetric analysis (TGA) of the samples was conducted using a TG 209F1 instrument (Netzsch, Germany) under an Ar atmosphere. The measurements were performed from room temperature to 600°C, with a heating rate of 10°C/min.

UV–Vis analysis

The optical properties of the samples were characterized by measuring their UV–Vis absorption spectra using a V-760 UV–Visible Spectrophotometer (Jasco). For solid samples, UV–Vis diffuse reflectance spectra were recorded in the wavelength range of 200–800 nm. In the case of film samples, UV–Vis-NIR spectra were obtained in the wavelength range of 200–1400 nm.

Differential scanning calorimetry (DSC)

The powder samples were assessed by DSC diagrams on a DSC204F1 (NETZSCH, Germany) with the conditions of room temperature to 300°C, a heating rate of 10°C/min, and nitrogen environment (Fig. 1).

Film hardness

The ability of coatings to endure everyday conditions, including resistance to scratches, is a crucial physical property. The pencil hardness test is a widely employed and straightforward method to evaluate this property. It follows the ASTM D3363 Pencil Hardness Test Method, which measures the resistance of a dry paint film surface against damage caused by friction from a sharp-pointed object with a known hardness, resulting in a scratch. The underlying principle of the pencil hardness test is based on the fact that a harder material will scratch a surface with a lower hardness.

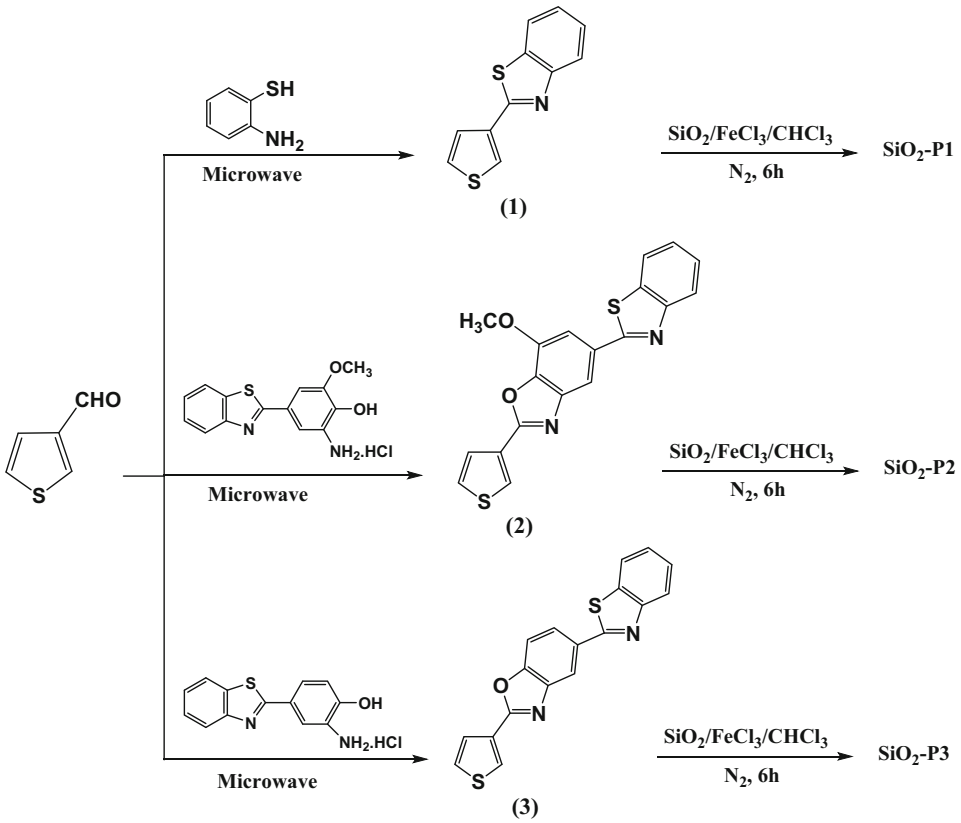

Fig. 1: Synthetic procedure of thiophene monomers and the polythiophene/SiO_2 nanocomposites

Abrasion resistance test

The falling sand abrasion resistance test is employed to assess the resistance of organic coatings against abrasion. The test was conducted using a Falling Sand Abrasion Tester in accordance with the ASTM D968-15 standard. The results of the test are expressed in L/mil, where 1 mil is equivalent to 25.4 μm. The abrasion resistance is calculated based on the volume of sand (V) and the thickness of the coating (d), using a specific formula:

$$\text{Abrasion resistance} = \frac{V}{d}(\text{L/mil}) \quad (1)$$

Accelerated weathering test

The accelerated weathering test was conducted using an Atlas UV-CON model 372 equipped with a UV-340 lamp (wavelength of 340 nm, intensity of 0.89 W/m^2/nm). This test was performed in accordance with ASTM G154-12 standards, involving a cycle weathering test comprising 8 h of UV exposure at 60°C (±3°C) followed by 4 h of water condensation at 50°C (±3°C). Subsequently, all samples were subjected to further tests and analysis after being completely dried at 50°C in a vacuum oven until reaching a constant weight. They were then conditioned at 25°C and 50% relative humidity for at least 24 h before further analysis.

The changes in the investigated samples during the accelerated weathering test were evaluated based on chemical changes using IR spectroscopy (Nicolet iS10, Thermo Scientific, USA), gloss measurements (Erichsen model 503), and weight changes.

Results and discussion

Characteristics and properties of nanocomposite based on SiO_2 and polythiophenes' derivations

Fourier transform infrared spectra analysis (FTIR)

The FTIR spectra in Fig. 2 show characteristic peaks of functional groups of SiO_2 and polythiophenes in the synthesized nanocomposite and SiO_2 nanoparticles. The FTIR spectra of the nanocomposites exhibited the asymmetry and symmetry stretching vibrations of the Si-O-Si linkage at wavenumbers of 1150 cm^{-1} and 840 cm^{-1}, respectively, while the Si-O-Si bending vibration was observed at 500 cm^{-1}. Additionally, the stretching vibration of the O-H linkage was assigned at 3400 cm^{-1}.[30] The vibration corresponding to the Si-O-Si linkage in the nanocomposites appeared at the same

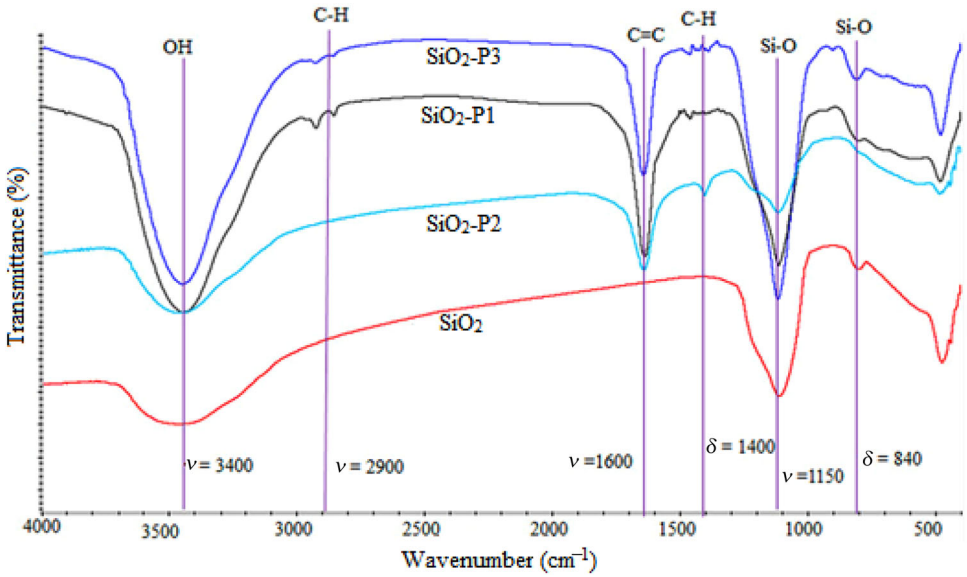

Fig. 2: FTIR spectra of SiO_2 modified with polythiophenes

position as that of the SiO_2 nanoparticles in their FTIR spectra. However, there were noticeable differences between the FTIR spectra of the nanocomposites and pure nanosilica. Specifically, the stretching vibration associated with the C=C–C=C conjugate circuit, which is characteristic of the thiophene ring, was observed at 1600 cm^{-1}. The bending vibration of the C–H linkage in the thiophene and benzene rings (=C–H) was assigned at 1400 cm^{-1}. Another observed stretching vibration at 1468 cm^{-1} indicated the presence of the C=N bond in the conjugated ring system.[1,25] These findings confirm the successful polymerization and grafting of polythiophenes onto the surface of SiO_2 nanoparticles. The increased absorbance intensity of the O-H peak could be attributed to the moisture absorption ability of polythiophenes in the nanocomposites.

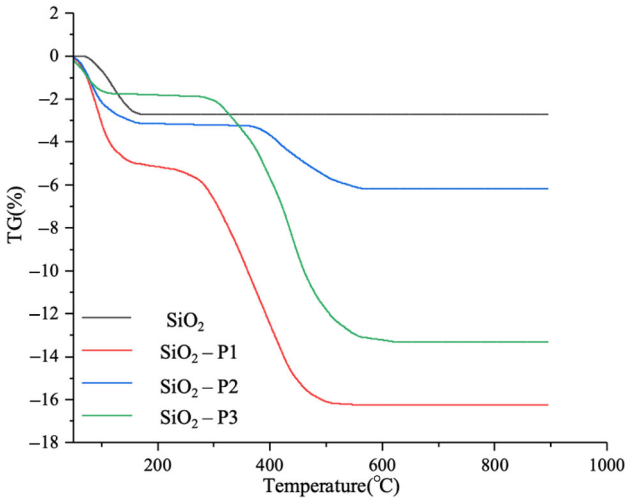

Fig. 3: TG diagrams of SiO_2 nanoparticles and SiO_2-based nanocomposites

Thermal properties

Figure 3 presents the TG diagrams illustrating the thermal behavior of the SiO_2 nanoparticles and SiO_2-based nanocomposites. It is evident from the graph that the SiO_2 nanoparticles exhibit remarkable thermal stability. The weight reduction of 2.69% observed below 180°C can be attributed to the loss of humidity and adsorbed water molecules from the nanosilica.[31] On the other hand, the SiO_2-based nanocomposites exhibit two distinct degradation stages. The first stage corresponds to the loss of humidity and water molecules, which is similar to the behavior observed in the SiO_2 nanoparticles (indicated as T_{max1} on the DrTG diagrams). The second stage arises from the decomposition of polymers, involving the breakage of C-C chains in the nanocomposites (indicated as T_{max2} on the DrTGA diagrams).

The TG analysis results indicate that the nanocomposites exhibited distinct degradation behavior in comparison with the SiO_2 nanoparticles. The weight loss of the nanocomposites occurred at lower temperatures, potentially due to the moisture absorption capacity of the polythiophenes within the nanocomposites. At higher temperatures, the polythiophenes underwent degradation, resulting in the formation of smaller molecular weight substances such as oligomers, monomers, CO_2, and H_2O.[1,27] The degradation of the polythiophenes led to a decrease in the π-conjugation effect and an increase in the spatial arrangement of the polymer side chains. Completed decomposition of the polythiophenes occurred at temperatures ranging from 500 to 550°C, depending on their specific structures. The remaining mass at temperatures above 600°C was

attributed to the SiO_2 nanoparticles, which demonstrated high thermal stability.[31] These findings confirm the successful formation of polythiophenes on the surface of the nanosilica.

The results highlight that the thermal stability of the polythiophenes can be significantly influenced by their structural characteristics. The enhanced thermal stability observed in P2 and P3 may be attributed to factors such as the presence of bulky substituents or the length of the conjugated chain in their chemical structures. The lower weight loss observed for P3 at higher temperatures suggests its suitability for high-temperature applications. Additionally, the estimated weight of P2 and P3 in the nanocomposites is higher compared to P1, indicating a greater adsorption of P2 and P3 molecules onto the surface of the SiO_2 nanoparticles compared to P1. This discrepancy may arise from the distinct chemical structures of the polymers, affecting their interaction with the SiO_2 surface.

Morphology

Figure 4 displays the SEM images depicting the morphology of SiO_2 nanoparticles and SiO_2-based nanocomposites. The images reveal that the nanocomposites exhibit a morphology similar to that of the SiO_2 nanoparticles. However, they differ from the polymers synthesized using surfactants, as reported previously.[27] Importantly, the polymerization process did not cause any significant alterations in the size and shape of the nanosilica nanoparticles.

To more clearly observe the structural morphology of the nanocomposites, HR-TEM technique has been used to conduct the morphology of SiO_2-P3 nanocomposite and the results are presented in Fig. 5. It can be seen that the SiO_2-P3 nanocomposite exhibits a spherical shape with relatively small sizes, ranging from 10 to 20 nm. However, these particles tend to agglomerate together to form larger-sized particles. The spherical morphology of the SiO_2-P3 particles indicates a uniform and well-defined structure. The presence of a thin layer of polythiophene on the surface of the SiO_2 nanoparticles is evident from the observed boundaries between the nanoparticles. It not only confirms the successful synthesis of the SiO_2-P3 nanocomposite but also suggests the formation of a hybrid material with enhanced properties through in situ reaction.

UV–Vis spectroscopy

Figure 6 illustrates the UV–Vis spectra of SiO_2 nanoparticles and SiO_2-based nanocomposites dispersed in distilled water. The spectra demonstrate that

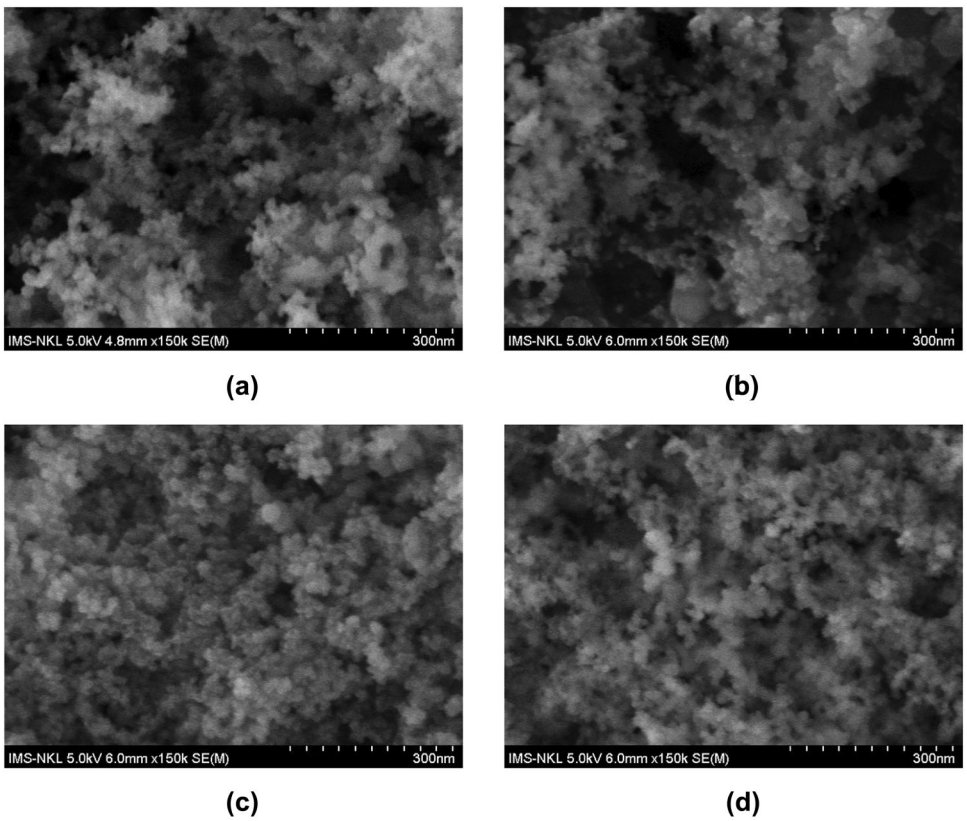

Fig. 4: SEM images of SiO_2 (a) and SiO_2-based nanocomposites, SiO_2-P1 (b), SiO_2-P2 (c), and SiO_2-P3 (d)

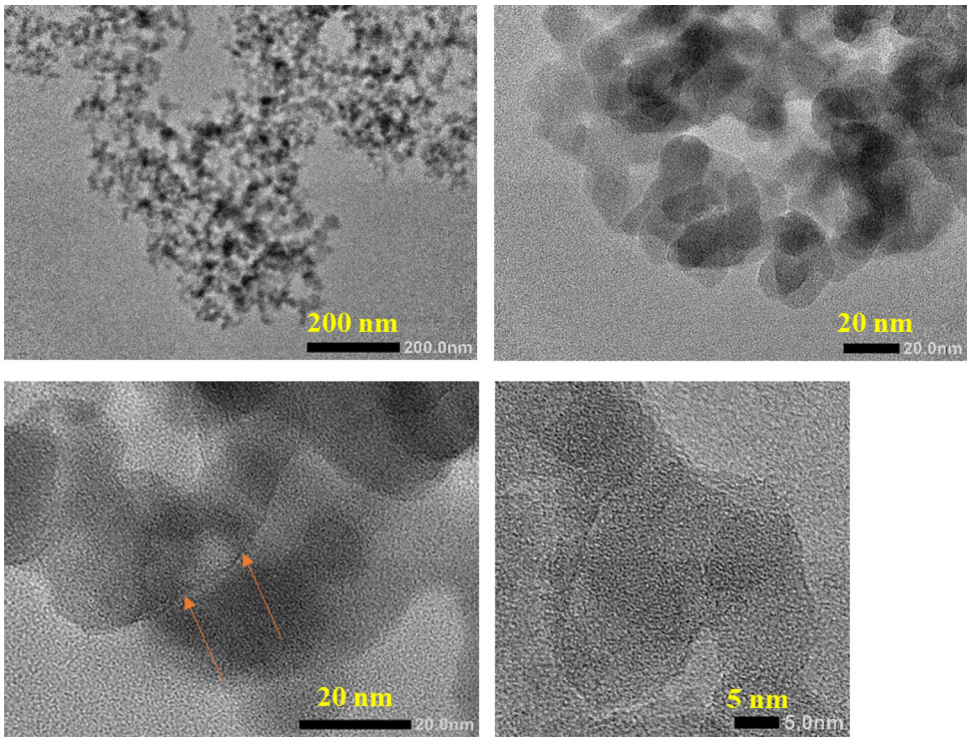

Fig. 5: HR-TEM images of SiO_2-P3 nanocomposite

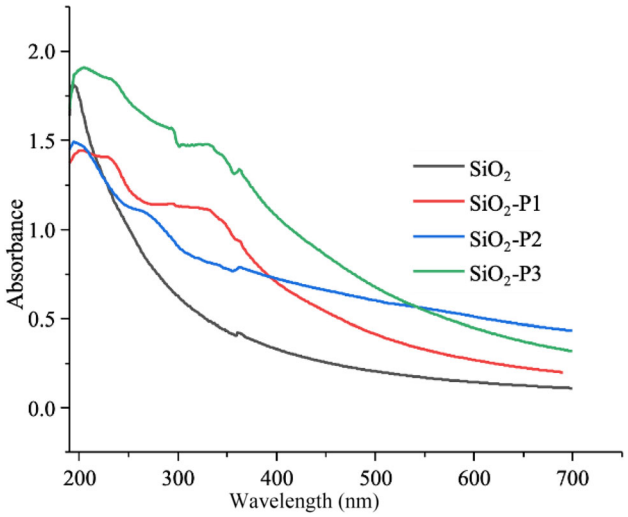

Fig. 6: UV–Vis spectra of nanocomposite

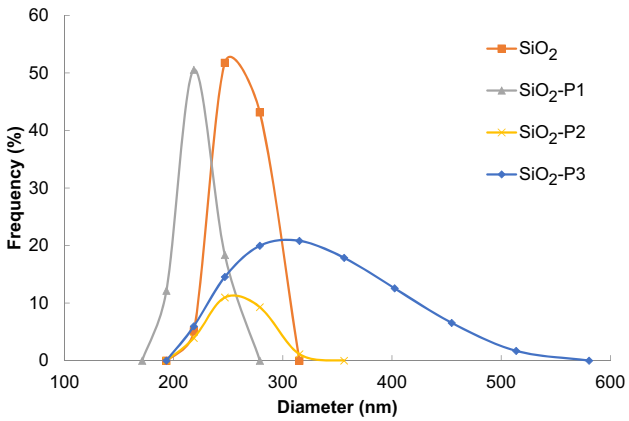

Fig. 7: Size distribution of SiO_2 and SiO_2-based nanocomposites, SiO_2-P1, SiO_2-P2, and SiO_2-P3

the nanosilica particles absorb UV rays at a wavelength of 200 nm. Furthermore, the SiO_2-based nanocomposites exhibit a UV absorption maximum between 203 and 210 nm.[32,33] As polythiophenes also absorb UV rays within the wavelength range of 300–400 nm,[27] the UV absorption peak of the SiO_2-based nanocomposites becomes broadened due to the interaction between the nanosilica and polythiophenes. The great absorption ability of SiO_2-based nanocomposites in the visible region may be due to the presence of the benzo[d]thiazole ring in PThs on the surface of nanosilica. Among the three investigated SiO_2-based nanocomposites, the SiO_2-P3 demonstrates the highest UV absorption, indicating that the P3 exhibits the strongest interaction with the nanosilica.

Size distribution and Zeta potential

Figure 7 presents the size distribution diagrams of nanosilica particles and SiO_2-based nanocomposites dispersed in water, with a polydispersity index (PDI) of less than 1. The average particle size value was found to be larger than the peak size value, indicating that the

nanocomposites exhibited a polydisperse distribution in water.

Nanosilica particles exhibited excellent dispersion in water, with a size distribution ranging from 218.6 to 315.27 nm. The effective dispersion of nanosilica in water can be attributed to the abundance of hydroxyl groups situated on the surface of the particles, rendering them hydrophilic in nature.[32,33] However, the nanocomposites displayed a higher hydrophobicity property compared to the nanosilica due to the presence of polythiophenes on their surface, resulting in a reduction in the number of hydroxy groups, causing the poor dispersion of the nanocomposites in the aqueous environment, leading to larger average particle size of the nanocomposites as compared to that of the silica nanoparticles. The difference in the peak size and average particle size of the SiO_2-based nanocomposites may be attributed to the structural differences of the polythiophenes P1, P2, and P3.

Following the modification with polythiophenes, the surface charge of the nanosilica particles was shifted from negative to positive, as indicated in Table 1. This change can be attributed to the conductive nature of polythiophenes, which can become cations in aqueous media, resulting in a positive surface charge for the nanocomposites. A high surface charge, above + 30 mV or below − 30 mV, also signifies a hydrodynamic stable system in water. The findings in Table 1 demonstrate that the hydrodynamic stability in water of SiO_2, SiO_2-P1, and SiO_2-P3 samples is great and it was ordered as SiO_2-P2 < SiO_2-P3 < SiO_2 < SiO_2-P1.

DSC result

Figure 8 presents the DSC diagrams of SiO_2, polymer P3, SiO_2-P3 (in situ), and SiO_2-P3-mix (mechanical mixing of SiO_2 and polymer P3). It can be seen that SiO_2 does not exhibit any effects in temperature ranging from room temperature to 300°C. Polymer P3 exhibits an endothermic effect at 63.7°C with an enthalpy of 41.22 J/g, corresponding to the loss of humidity and absorbed water in the polymer P3. For SiO_2-P3 nanocomposite that synthesized through an in situ process, the differences between two DSC diagrams of P2 and SiO_2-P3 are significant. The SiO_2-P3 nanocomposite exhibits two endothermic peaks at 60.5°C and 136.7°C, corresponding to the loss of water

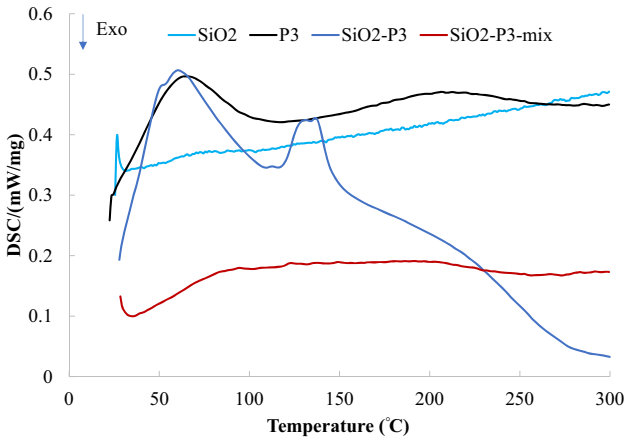

Fig. 8: DSC diagrams of SiO_2, polymer P3, SiO_2-P3 (in situ), and SiO_2-P3 (mixture)

in SiO_2 and polymer P3. The total enthalpy for this process is 115.1 J/g. In the case of SiO_2-P3-mix that was mixed mechanically, there is no effect observed in the temperature ranging from room temperature to 300°C. These results confirm the successful synthesis of SiO_2-P3 nanocomposite through in situ process.

Effect of SiO_2-based nanocomposites on acrylic coatings

Effect of polythiophenes derivation on mechanical properties of acrylic coatings

Table 2 demonstrates the effect of SiO_2 nanocomposites on the abrasion resistance and hardness of the acrylic coating. Remarkably, the SiO_2-P3 nanocomposite exhibited a significant improvement in both abrasion resistance and hardness. This enhancement can be attributed to several factors: Firstly, the high polymerization yield of P3 on the SiO_2 reduces nanosilica agglomeration by promoting intermolecular hydrogen bonding between the hydroxyl groups on the nanosilica surface, resulting in a regular dispersion of nanocomposite particles within the polymer resin. Secondly, polymer P3 possesses a longer hydrocarbon chain length and lacks branched circuits, preventing space obstruction when formed on the nanosilica surface and dispersed in the acrylic emulsion resin.

Table 1: Size distribution, average particle size, PDI, and zeta potential of SiO_2 and SiO_2-based nanocomposites

No.	Sample	Peak size (nm)	Average particle size (nm)	PDI	Zeta potential (mV)
1	SiO_2	244.0	287.0 ± 5.7	0.349	− 81.4
2	SiO_2-P1	208.2	373.7 ± 10.2	0.424	114.8
3	SiO_2-P2	242.1	464.8 ± 18.6	0.513	37.2
4	SiO_2-P3	304.0	427.5 ± 15.5	0.427	67.2

Table 2: Abrasion resistance and hardness of acrylic resin-based coatings containing different SiO_2-based nanocomposites

Sample	Abrasion resistance (L/mil)	Film hardness (Pencil hardness)
Acrylic	80.0 ± 1.6	HB
Acrylic/SiO_2-P1-5%	98.0 ± 2.1	F
Acrylic/SiO_2-P2-5%	90.0 ± 1.5	F
Acrylic/SiO_2-P3-5%	110.0 ± 1.8	1H

Thirdly, the polymer P3 acts as a bridge between the polymer resin and nanosilica, enhancing their interaction and contributing to improved mechanical properties. Lastly, the excellent water dispersibility of SiO_2-P3, as observed in the size distribution analysis, enables its effective dispersion in the acrylic emulsion resin. Collectively, these factors synergistically contribute to the notable enhancement of abrasion resistance and hardness achieved by the SiO_2-P3 nanocomposite in the acrylic coating.

Therefore, considering the characteristics of SiO_2-based nanocomposites and the enhanced abrasion resistance and pencil hardness of the acrylic/nanocomposite coating, we have selected the SiO_2-P3 nanocomposite for further exploration of the properties in the acrylic-based coating.

Effect of SiO_2-P3 content on mechanical properties of acrylic coatings

We have evaluated the impact of varying contents (1, 2, 3, and 5 wt.%) of SiO_2-P3 nanocomposite, in comparison with the weight of the solid resin, on the abrasion resistance of acrylic-based coatings. The results of this evaluation are presented in Table 3.

The results presented in Table 3 clearly demonstrate that the content of SiO_2-P3 nanocomposite significantly influenced the abrasion resistance of the acrylic coating. Surprisingly, the addition of nanosilica did not enhance the abrasion resistance as anticipated. This finding aligns with a previous study by other authors.[20,34] The lack of improvement can be attributed to the agglomeration of nanosilica particles, which is caused by intermolecular hydrogen bonding between the hydroxyl groups on the surface of the nanosilica. As a result, the nanosilica is unevenly dispersed within the acrylic resin matrix, leading to defects in the microstructure of the coating and reduced resistance to external physical forces. Consequently, the abrasion resistance of the acrylic/SiO_2-2% coating was diminished.

In contrast, it was observed that the SiO_2-P3 nanocomposite serves as a reinforcing additive for acrylic coatings, particularly when incorporated up to a content of 3 wt.%. The introduction of nanocomposite particles into the coating system facilitates interaction between the organically functional groups of polythiophene within the nanocomposite and the acrylate groups present in the acrylic emulsion resin. This interaction promotes a uniform dispersion of the nanocomposite within the polymer matrix. As a result, the coatings exhibit enhanced durability and improved resistance to external physical forces.[19,35,36]

The abrasion resistance of acrylic-based coatings exhibited an increase as the nanocomposite content was raised from 1 to 2 wt.%, but gradually decreased thereafter. The percentage of nanoparticles introduced plays a significant role in determining the properties of the coating film. When an appropriate particle ratio is utilized, it promotes favorable phase interaction with the acrylic resin, allowing the nanocomposite particles to effectively interlock with the polymer chains of the acrylic resin. Consequently, the coating's structure becomes denser and more durable. However, the coating containing 5 wt.% of SiO_2-P3 nanocomposite

Table 3: Abrasion resistance and film hardness of acrylic resin-based coatings containing different SiO_2-P3 nanocomposite contents

Sample	Abrasion resistance (L/mil)	Pencil hardness
Acrylic	80.0 ± 1.6	HB
Acrylic/SiO_2-2%	67.0 ± 4.7	F
Acrylic/SiO_2-P3-1%	136.7 ± 6.2	2H
Acrylic/SiO_2-P3-2%	171.3 ± 5.1	2H
Acrylic/SiO_2-P3-3%	128.7 ± 5.8	2H
Acrylic/SiO_2-P3-5%	110.0 ± 1.8	1H

demonstrated low abrasion resistance (110.0 ± 1.8 L/mil). This can be attributed to the excessive amount of nanocomposite particles, leading to their aggregation and the formation of defects in the coating's microstructure. Furthermore, this agglomeration hampers the interaction between the groups in the SiO_2-P3 nanocomposite and the groups in the acrylic resin, as well as interferes with the resin crosslinking process. As a result, the coating exhibits reduced abrasion resistance.

Table 3 clearly demonstrates that the acrylic coating without additives exhibits the lowest hardness (HB). Comparatively, at the same additive content, SiO_2-P3 exhibits a more pronounced positive effect on enhancing the hardness of the acrylic resin compared to SiO_2 nanoparticles. This confirms that the modification of nanosilica with polythiophene contributes significantly to the improvement of the mechanical properties of the acrylic coating. The observed enhancement in hardness can also be attributed to the improved dispersion of the SiO_2-P3 nanocomposite within the acrylic matrix, as mentioned earlier. Furthermore, the content of SiO_2-P3 demonstrates a marginal impact on the hardness of the acrylic coatings. This can be explained by the fact that these nanocomposites possess a spatial polymer structure (network polymer) that is tightly interconnected, thereby affecting stiffness more prominently than the amorphous structure of the silica nanoparticles.

Morphology of acrylic-based nanocomposite coatings

Figure 9 depicts the SEM images of the acrylic/SiO_2-P3-2% and acrylic/SiO_2-2% coatings, revealing the hetero-microstructure of the acrylic-based coatings. The poor dispersion of silica nanoparticles in the acrylic matrix is evident due to aggregation, attributed to intermolecular hydrogen bonding of hydroxyl groups on the nanosilica surface (Fig. 9a). Following modification with polythiophene, SiO_2-P3 demonstrates a uniform dispersion within the polymer matrix (Fig. 9b), facilitated by polythiophene acting as a bridge between nanoparticles and the polymer matrix, enhancing dispersibility of SiO_2-P3 nanocomposite in the acrylic coating. This improved dispersion is further highlighted in the SEM images of the cross section of the acrylic-based coatings in Figs. 9c and 9d. While SiO_2-P3 tends to agglomerate in the acrylic matrix, cluster size is notably smaller than that of SiO_2 nanoparticles. Upon impact, microholes appear on the microstructure of the acrylic/SiO_2-2% coating, indicating that large clusters of SiO_2 nanoparticles in acrylic serve as stress points. In contrast, SiO_2-P3 dispersed in the acrylic coating forms a regular and stable structure for the nanocomposite coating, contributing to the enhancement of mechanical properties in acrylic coatings as mentioned earlier.

Thermal stability of acrylic-based nanocomposite coatings

Figure 10 reveals that the presence of nanosilica and SiO_2-P3 nanocomposite slightly increased the onset temperature of thermal decomposition of the nanocomposite coating. This effect can be attributed to the nanoscale influence of nanosilica within the polymer matrix, as reported in previous studies.[20,34,35] The weight loss of the coatings primarily occurred in the range of 300–400°C, resulting from the polymer chains breaking under the impact of heat.[34–37] Upon heating, the acrylic resin decomposed into low-molecular-weight organic substances, carbon, and water. Since the weight of nanosilica in the coatings was small, the resulting char residue was negligible. Despite polythiophenes having moderate thermal stability, the modification of nanosilica with polythiophenes did not significantly impact the thermal degradation of the acrylic emulsion resin. This observation can be attributed to the uniform dispersion of the SiO_2-P3 nanocomposite within the acrylic resin matrix, as discussed earlier.

Effect of SiO_2-based nanocomposite on weathering durability of acrylic coating

FTIR analysis

The results obtained from the IR spectra of the AC, AC/SiO_2, and AC/SiO_2-P3 coatings before and after weathering indicate that exposure to UVA rays impacts the coating surface, leading to changes in the coating film. Consequently, after the aging test and subsequent measurement of the samples, a significant reduction is observed in the spectral pattern of the CH and C=O groups compared to the original sample (Fig. 11). Based on the results obtained from IR spectroscopy, the change in the carbonyl index (CI) can be calculated by determining the ratio of the characteristic peak area corresponding to the vibration of the CH group to the characteristic peak area corresponding to the fluctuation of the C=O group.

Figure 12 illustrates the impact of UV light on the coating films. During the accelerated weathering test, the paint film is exposed to ultraviolet radiation, oxygen, air, moisture, and temperature. As a result, the quality of the paint film can deteriorate due to thermo-oxidative, photooxidative, and hydrolytic decomposition reactions.[19,38] These reactions directly influence the two primary functional groups in the AC coating composition, namely the carbonyl group and the CH group. The changes in these functional groups are clearly demonstrated through each irradiation cycle and measured using infrared spectroscopy equipment. It has been observed that when utilizing an appropriate nanocomposite content, the properties of the coating film are enhanced. In particular, the UV shielding ability of the 2 wt.% nanocomposite sample

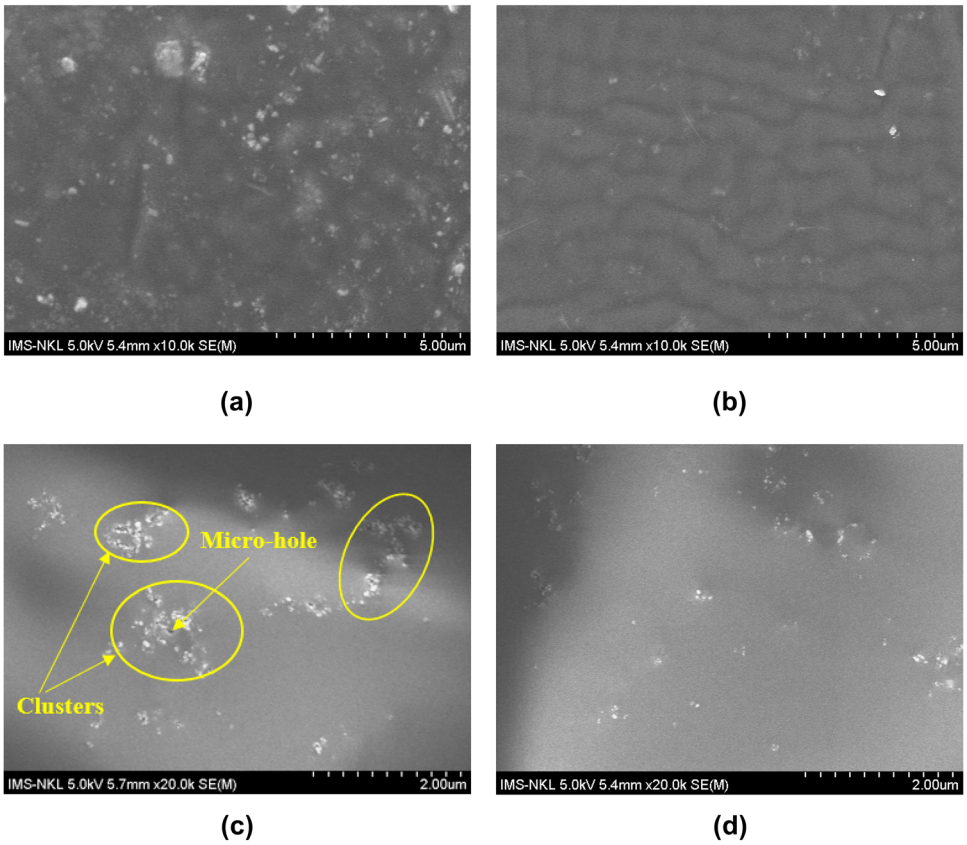

Fig. 9: SEM images of surface of acrylic/SiO_2-2% coating (a), acrylic/SiO_2-P3-2% coating (b) and cross surface of acrylic/SiO_2-2% coating (c), acrylic/SiO_2-P3-2% coating (d)

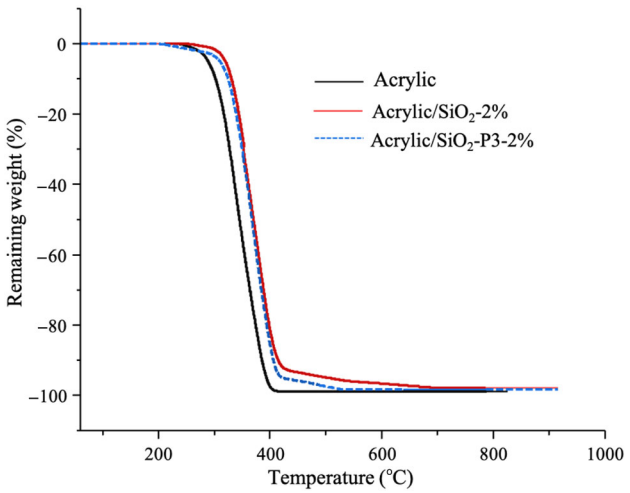

Fig. 10: TGA diagrams of acrylic-based coatings

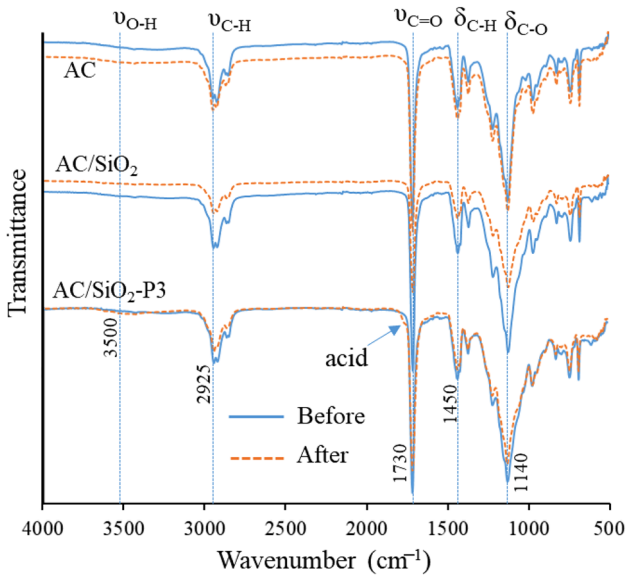

Fig. 11: FTIR spectra of neat coating (AC), nanocomposite coating containing 2 wt.% nano-SiO_2(AC/SiO_2), and nanocomposite coating containing 2 wt.% nanocomposite SiO_2-P3 (AC/SiO_2-P3) after 30 aging cycles (equal 360 h)

is the most effective, and both the C=O and CH indexes are reduced to the lowest levels. However, when increasing the particle content of the sample by 10 wt.%, the carbonyl index is decreased even more significantly. This can be attributed to the excessive

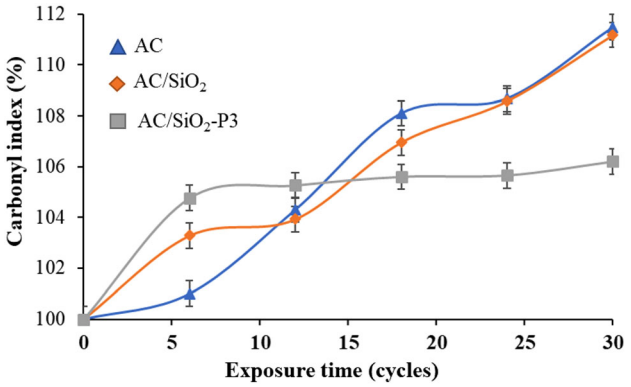

Fig. 12: Changes of CI upon weathering test of neat coating (AC), nanocomposite coating containing 2 wt.% nano-SiO_2(AC/SiO_2), and nanocomposite coating containing 2 wt.% nanocomposite SiO_2-P3 (AC/SiO_2-P3).

amount of particles, which can affect the structure of the coating film and consequently impact the UV shielding ability of the film.

Gloss measurement

The process of accelerated weathering testing, under the influence of UVA rays, has changed the coating surface over cycles. As a result, the gloss of the coatings decreases with each cycle. The gloss of the coating that reduced less indicates a good UV shielding ability. Figure 13 shows that, initially, the gloss of the grain-free plastic sample has the greatest gloss, but when it undergoes weather aging, the percentage of gloss of this plastic film is increasingly lower, considering both the processes found that samples containing 2 wt.% of nanocomposites had the best gloss. The factors affecting the gloss of the coating are the solids content, the higher the solids content, the opaquer the coating becomes, and the addition of nanoparticles increases the roughness of the paint film and increases the coating properties particles on the surface lead to enhanced diffuse reflection of the coating surface, thereby reducing the gloss of coating.[38]

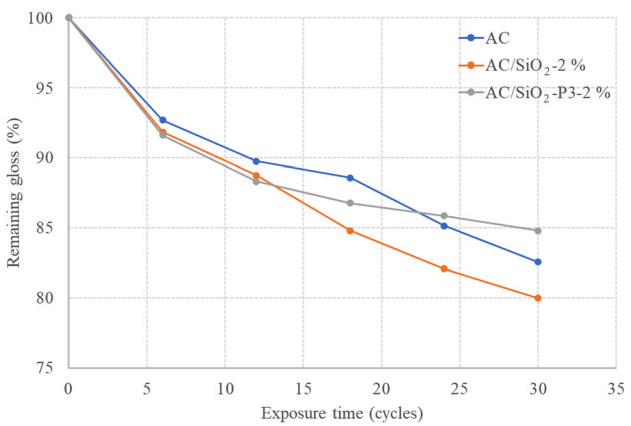

Fig. 13: Percent of the remaining gloss of AC coatings after weathering test

Weight loss of AC coatings

Following a weather acceleration test comprising 30 cycles, it became evident that the mass composition and structure of functional groups within the membrane changed when exposed to UVA rays. Specifically, after each cycle, a decrease in film weight was observed, indicating a clear change in the coating weight. As shown in Fig. 14, the residual weight percentage of the original resin sample was nearly 85%. In comparison, the sample containing 2 wt.% of silica nanoparticles exhibited a higher residual weight percentage of 90%, while the sample containing 2 wt.% of the nanocomposite AC/SiO_2-P3 had the lowest residual weight percentage of 95%. This phenomenon suggested that during the aging process under the influence of accelerated weathering factors such as ultraviolet radiation, oxygen, humidity, condensation, and heat, the bonds within the polymer chains could be broken through processes such as photolysis, photooxidation, photocatalysis, and hydrolysis.[18,38–42] Consequently, small quantities of other compounds such as CH_4, aldehydes, and alcohols were formed. These low-molecular-weight compounds may evaporate or be washed away during condensation, leading to a reduction in the coating's mass.

From the results above, a hypothesis mechanism can be suggested for the UV-resistance ability of AC, AC/SiO_2, and AC/SiO_2-P3 nanocomposites as shown in Fig. 15. When exposed to UV irradiation, the AC polymer chains undergo photodegradation, forming free radicals that result in defects in the microstructure of the AC coating, ultimately reducing the material's mechanical properties. In the presence of SiO_2

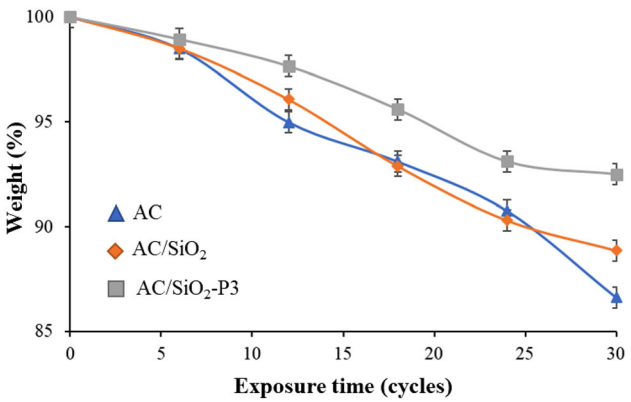

Fig. 14: Weight changes of coatings during the UV/CON aging of neat coating (AC), nanocomposite coating contained 2 wt.% nano-SiO_2(AC/SiO_2), and nanocomposite coating contained 2 wt.% nanocomposite SiO_2-P3 (AC/SiO_2-P3)

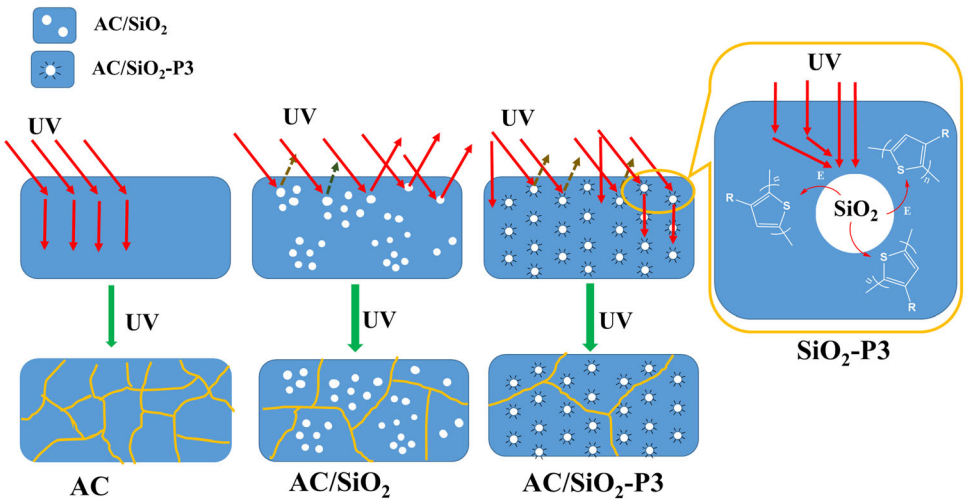

Fig. 15: Hypothesis mechanism for UV-resistance ability of AC, AC/SiO_2, and AC/SiO_2-P3 nanocomposites

nanoparticles, these particles can partially absorb UV rays, as illustrated in Fig. 6. The nanosilica also acts as a barrier, preventing UV rays from attacking the microstructure of the AC polymer and scattering the UV rays into the environment, thereby protecting the polymer during UV irradiation. However, the agglomeration of SiO_2 nanoparticles within the AC matrix limits their UV absorbance and shielding abilities, resulting in low protective effectiveness for the AC matrix. By introducing SiO_2-P3 nanocomposites into the AC matrix, their excellent dispersion allows them to significantly enhance the shielding ability of AC coatings. Additionally, they can both scatter and absorb UV rays, minimizing the impact of UV rays on the AC polymer chains. As a result, UV-absorbing materials can serve as photoprotectors for polymers, although the form in which the absorbed energy is converted and whether it is harmful to the polymer need to be evaluated. Therefore, it is essential to assess the products formed during photodegradation to establish a comprehensive working mechanism for these nanocomposites in UV-resistance.

Conclusions

This paper presents a novel coating based on acrylic emulsion resin and nanosilica modified with polythiophene derivatives. It is the first time the polythiophene derivatives have been used for modification of nanosilica. The IR, DLS, SEM, UV–Vis, and TGA analysis results have confirmed a successful modification of polythiophene derivatives containing benzo[*d*]thiazol heterocycle on the surface of nanosilica. The modification helps to broaden the visible light absorbance region of nanosilica. Interestingly, the addition of modified nanosilica contributed to not only the mechanical properties of acrylic coating but also its thermal properties and weather resistance. These results suggest that polythiophene derivatives are promising for modifying additives such as nanosilica, in particular, and inorganic nanoparticles, in general, to enhance the properties of organic coatings. This opens wide applications of polythiophene derivatives.

Author contributions NTTD was involved in preparation of nanocomposite and samples, investigation, and writing original draft; DBD contributed to preparation of nanocomposite and samples and conceptualization; NHT took part in preparation of nanocomposite and methodology; NTC participated in methodology and data analysis, supervision, and writing review and editing; NXT was responsible for methodology and investigation; DPH was involved in data analysis and writing original draft; TH contributed to writing review and editing and conceptualization; NNL took part in data analysis; VQM participated in preparation of samples and methodology; VQT was responsible for conceptualization and writing review and editing.

Conflict of interest The authors declare no competing interests.

References

1. Kaloni, TP, Giesbrecht, PK, Schreckenbach, G, "Polythiophene: From Fundamental Perspectives to Applications." *Chem. Mater.*, **29** (24) 10248–10283 (2017)
2. Chandrasekhar, P, *Conducting Polymer, Fundamentals and Applications*. Kluwer Academic Publishers, Boston, Dordrecht, London (1999)
3. Fichou, Dais, *Handbook of Oligo—and Polythiophene*. Wiley-VCH, Weinheim, New York, Chichester, Brisbane, Singapore, Toronto (1999)
4. Truong, VK, Stefanovic, M, Maclaughlin, S, Tobin, M, Vongsvivut, J, Al Kobaisi, M, Crawford, RJ, Ivanova, EP, "The Evolution of Silica Nanoparticle Polyester Coatings on

Surfaces Exposed to Sunlight.'' *J. Vis. Exp.*, **116** 54309–54325 (2016)
5. Wang, X, Cui, Y, Wang, Y, Ban, T, Zhang, Y, Zhang, J, Zhu, X, ''Preparation and Characteristics of Crosslinked Fluorinated Acrylate Modified Waterborne Polyurethane for Metal Protection Coating.'' *Prog. Org. Coat.*, **158** 106371 (2021)
6. Ji, S, Gui, H, Guan, G, Zhou, M, Guo, Q, Tan, MYJ, ''Molecular Design and Copolymerization to Enhance the Anti-corrosion Performance of Waterborne Acrylic Coatings.'' *Prog. Org. Coat.*, **153** 106140 (2021)
7. Wu, M, Ge, S, Jiao, C, Yan, Z, Jiang, H, Zhu, Y, Dong, B, Dong, M, Guo, Z, ''Improving Electrical, Mechanical, Thermal and Hydrophobic Properties of Waterborne Acrylic Resin- Glycidyl Methacrylate (GMA) by Adding Multi-walled Carbon Nanotubes.'' *Polymer*, **200** 122547 (2020)
8. Vu, Q-T, Pavlik, M, Hebestreit, N, Rammelt, U, Plieth, W, Pfleger, J, ''Nanocomposites Based on Titanium Dioxide and Polythiophene: Structure and Properties.'' *React. Funct. Polym.*, **65** (1–2) 69–77. https://doi.org/10.1016/j.reactfunctpolym.2004.11.011 (2005)
9. Vu, Q-T, Pavlik, M, Hebestreit, N, Pfleger, J, Rammelt, U, Plieth, W, ''Electrophoretic Deposition of Nanocomposites Formed from Polythiophene and Metal Oxides.'' *Electrochim. Acta*, **51** (6) 1117–1124. https://doi.org/10.1016/j.electacta.2005.05.052 (2005)
10. Li, H, Yang, Y, Yunzhao, Y, ''Acrylic Emulsion Pressure-Sensitive Adhesives (PSAS) Reinforced with Layered Silicate.'' *J. Adhesion Sci. Technol.*, **18** (15–16) 1759–1770. https://doi.org/10.1163/1568561042708340 (2004)
11. Márquez, I, Paredes, N, Alarcia, F, Velasco, JI, ''Adhesive Performance of Acrylic Pressure-Sensitive Adhesives from Different Preparation Processes.'' *Polymers (Basel)*, **13** (16) 2627. https://doi.org/10.3390/polym13162627 (2021)
12. Wu, J, Zhang, R, Li, P, et al. ''Synthesis of Fluorinated Polyacrylic Acrylate Oligomer for the UV-Curable Coatings.'' *J. Coat. Technol. Res.*, **16** 681–688. https://doi.org/10.1007/s11998-018-0145-5 (2019)
13. Pang, B, Ryu, C-M, Jin, X, Kim, H-I, ''Preparation and Properties of UV Curable Acrylic PSA by Vinyl Bonded Graphene Oxide.'' *Appl. Surf. Sci.*, **285** 727–731. https://doi.org/10.1016/j.apsusc.2013.08.117 (2013)
14. Perera, DY, ''Effect of Pigmentation on Organic Coating Characteristics.'' *Prog. Org. Coat.*, **50** (4) 247–262 (2004)
15. Khalina, M, Sanei, M, Mobarakeh, HS, Mahdavian, AR, ''Preparation of Acrylic/Silica Nanocomposites Latexes with Potential Application in Pressure Sensitive Adhesive.'' *Int. J. Adhes. Adhes.*, **58** 21–27. https://doi.org/10.1016/j.ijadhadh.2014.12.007 (2015)
16. Xu, C-A, Qu, Z, Meng, H, Chen, B, Wu, X, Cui, X, Wang, K, Wu, K, Shi, J, Lu, M, ''Effect of Polydopamine-Modified Multi-walled Carbon Nanotubes on the Thermal Stability and Conductivity of UV-Curable Polyurethane/Polysiloxane Pressure-Sensitive Adhesives.'' *Polymer*, **223** 123615. https://doi.org/10.1016/j.polymer.2021.123615 (2021)
17. Ramezanzadeha, B, Moradiana, S, Tahmasebi, N, Khosravi, A, ''Studying the Role of Polysiloxane Additives and Nano-SiO_2 on the Mechanical Properties of a Typical Acrylic/Melamine Clearcoat.'' *Prog. Org. Coat.*, **72** (4) 621–631 (2011)
18. Yari, H, Moradian, S, Tahmasebi, N, ''The Weathering Performance of Acrylic Melamine Automotive Clearcoats Containing Hydrophobic Nanosilica.'' *J. Coat. Technol. Res.*, **11** (3) 351–360 (2014)
19. Nguyen, TV, Nguyen, TA, Nguyen, TH, ''The Synergistic Effects of SiO_2 Nanoparticles and Organic Photostabilizers for Enhanced Weathering Resistance of Acrylic Polyurethane Coating.'' *J. Compos. Sci.*, **4** (1) 23 (2020)
20. Zhou, S, Wu, L, Sun, J, Shen, W, ''The Change of the Properties of Acrylic-Based Polyurethane via Addition of Nano-silica.'' *Prog. Org. Coat.*, **45** 33–42 (2002)
21. Park, SJ, Cho, KS, ''Filler- Elastomer Interactions: Influence of Silane Coupling Agent on Crosslink Density and Thermal Stability of Silica/Rubber Composites.'' *J. Colloid Interface Sci.*, **267** 86–91 (2003)
22. Stojanovic, D, Orlovic, A, Markovic, S, Radmilovic, V, Uskokovic, PS, Aleksic, R, ''Nanosilica/PMMA Composites Obtained by the Modification of Silica Nanoparticles in a Supercritical Carbon Dioxide–Ethanol Mixture.'' *J. Mater. Sci.*, **44** 6223–6232. https://doi.org/10.1007/s10853-009-3842-8 (2009)
23. Lv, X, Wang, J, Guo, Y, et al. ''Preparation of UV-Curable Nano-SiO_2/ Acrylate Coatings Modified by P-Containing LEPB and Their Applications on Plywood.'' *J. Coat. Technol. Res.*, **20** 2031–2044. https://doi.org/10.1007/s11998-023-00799-y (2023)
24. Zhang, J, Hongping, X, Ling, H, Yang, Y, Li, H, Huang, C, Liu, X, ''Novel Waterborne UV-Curable Hyperbranched Polyurethane Acrylate/Silica with Good Printability and Rheological Properties Applicable to Flexographic Ink.'' *ACS Omega*, **2** (11) 7546–7558 (2017)
25. Gong, X, He, S, ''Highly Durable Superhydrophobic Polydimethylsiloxane/Silica Nanocomposite Surfaces with Good Self-Cleaning Ability.'' *ACS Omega*, **5** (8) 4100–4108 (2020)
26. Lin, B, Zhou, S, ''Poly(ethylene glycol)-Grafted Silica Nanoparticles for Highly Hydrophilic Acrylic-Based Polyurethane Coatings.'' *Prog. Org. Coat.*, **106** 145–154. https://doi.org/10.1016/j.porgcoat.2017.02.008 (2017)
27. Duong, TTT, Linh, NN, Manh, VQ, Hien, HTT, Dai, DB, Hien, N, Chinh, NT, Linh, DK, Hung, HM, Duc, LM, Hoang, T, Oanh, DTY, Trung, VQ, ''Synthesis and Properties of Some Polythiophenes Containing Benzo[d]thiazole Heterocycle.'' *VNU J. Sci.: Natl. Sci. Technol.*, **38** 4. https://doi.org/10.2507/2588-1140/vnunst.5376 (2022)
28. Nguyen Ngoc, L, Vu Quoc, T, Duong Quoc, H, Vu Quoc, M, Truong Minh, L, Thang Pham, C, Van Meervelt, L, ''Green Synthesis and Crystal Structure of 3-(Benzo-thia-zol-2-yl)thio-phene.'' *Acta Cryst.*, **E73** 1647–1651. https://doi.org/10.1107/S2056989017014530 (2017)
29. Quoc, TV, Ba, DD, Thuy, DTT, Ngoc, LN, Thuy, CN, Thi, HV, Khanh, LD, Yen, ODT, Thai, H, Long, VC, Talu, S, Trong, DN, ''DFT Study on Some Polythiophenes Containing Benzo[*d*]thiazole and Benzo[*d*]oxazole: Structure and Band Gap.'' *Designed Monomers Polym.*, **24** (1) 274–284. https://doi.org/10.1080/15685551.2021.1971376 (2021)
30. Kumari, A, Singh, RK, Kumar, N, Kumari, R, Sharma, S, ''Green Synthesis and Physical Properties of Crystalline Silica Engineering Nanomaterial from Rice Husk (Agriculture Waste) at Different Annealing Temperatures for Its Varied Applications.'' *J. Indian Chem. Soc.*, **100** (5) 100982. https://doi.org/10.1016/j.jics.2023.100982 (2023)
31. Zhang, H, Li, C, Guo, J, Zang, L, Luo, J, ''In Situ Synthesis of Poly(methyl methacrylate)/SiO_2 Hybrid Nanocomposites via 'Grafting Onto' Strategy Based on UV Irradiation in the Presence of Iron Aqueous Solution.'' *J. Nanomater.*,. https://doi.org/10.1155/2012/217412 (2012)
32. Meftah, N, Hani, A, Merdas, A, ''Extraction and Physico-chemical Characterization of Highly-pure Amorphous Silica Nanoparticles from Locally Available Dunes Sand.'' *Chem. Africa*,. https://doi.org/10.1007/s42250-023-00688-2 (2023)
33. Panwar, K, Jassal, M, Agrawal, AK, ''In Situ Synthesis of Ag–SiO_2 Janus Particles with Epoxy Functionality for

Textile Applications.'' *Particuology*, **19** 107–112. https://doi.org/10.1016/j.partic.2014.06.007 (2015)
34. Dao, PH, Nguyen, TV, Dang, MH, Nguyen, TL, Trinh, VT, Mac, VP, Nguyen, AH, Duong, M, ''Effect of Silica Nanoparticles on Properties of Coatings Based on Acrylic Emulsion Resin.'' *Vietnam J. Sci. Technol.*, **56** (3) 117–125 (2018)
35. Chen, G, Zhou, S, Gu, G, Wu, L, ''Modification of Colloidal Silica on the Mechanical Properties of Acrylic Based Polyurethane/Silica Composites.'' *Colloids Surf. A Physicochem. Eng. Aspects*, **296** 29–40 (2007)
36. Ettlinger, M, Ladwing, T, Weise, A, ''Surface Modified Fumed Silicas for Modern Coatings.'' *Prog. Org. Coat.*, **40** 31–34 (2000)
37. Jiang, ZX, Meng, LH, Huang, YD, Liu, L, Lu, C, ''Influence of Coupling Agent Chain Length on Interfacial Performance of Polyacrylacetylene Resin and Silica Glass Composites.'' *Appl. Surf. Sci.*, **253** 4338–4343 (2007)
38. Bui, TMA, Nguyen, TV, Nguyen, TM, Hoang, TH, Nguyen, TTH, Lai, TH, Tran, TN, Nguyen, VH, Hoang, VH, Le, TL, Tran, DL, Dang, TC, Vu, QT, Nguyen-Tri, P, ''Investigation of Crosslinking, Mechanical Properties and Weathering Stability of Acrylic Polyurethane Coating Reinforced by SiO_2 Nanoparticles Issued from Rice Husk Ash.'' *Mater. Chem. Phys.*, **241** 122445 (2020)
39. Nguyen, TV, Nguyen, TP, Nguyen, TD, Aidani, R, Trinh, VT, Decker, C, ''Accelerated Degradation of Water Borne Acrylic Nanocomposites Used in Outdoor Protective Coatings.'' *Polym. Degrad. Stab.*, **128** 65–76 (2016)
40. Nikolic, M, Nguyen, HD, Daugaard, AE, Lof, D, Mortensen, K, Barsberg, S, Sanadi, AR, ''Influence of Surface Modified Nano Silica on Alkyd Binder Before and After Accelerated Weathering.'' *Polym. Degrad. Stab.*, **126** 134–143. https://doi.org/10.1016/j.polymdegradstab.2016.02.006 (2016)
41. Fernández-Alvarez, M, Velasco, F, Bautista, A, Lobo, FCM, Fernandes, EM, Reis, RL, ''Manufacturing and Characterization of Coatings from Polyamide Powders Functionalized with Nanosilica.'' *Polymers*, **12** (10) 2298. https://doi.org/10.3390/polym12102298 (2020)
42. Jacques, LFE, ''Accelerated and Outdoor/Natural Exposure Testing of Coatings.'' *Prog. Polym. Sci.*, **25** (9) 1337–1362. https://doi.org/10.1016/S0079-6700(00)00030-7 (2000)